Model-based optimal operation of heating tower heat pump systems

Shifang Huang[a, b], Xing Lu[b], Wangda Zuo[b], Xiaosong Zhang[a, *], Caihua Liang[a]

[a] School of Energy and Environment, Southeast University, Nanjing, 210096, PR China

[b] Department of Civil, Environmental and Architectural Engineering, University of Colorado Boulder, Boulder, CO 80309, U.S.A.

[*] Corresponding author. E-mail address: rachpe@seu.edu.cn (Xiaosong Zhang)

Abstract: In current applications of heating tower heat pumps (HTHPs), the systems tend to run with constant speed or fixed set points, which can be inefficient under varying weather data and building loads. To address this issue, this study proposes a model-based optimal operation of the HTHPs to achieve energy savings in both cooling and heating modes. Firstly, a physics-based model for an existing HTHP system was developed. Then, artificial neural network (ANN) models were developed and trained with vast amount of operational data generated by the physics-based model. The ANN models were found to be highly accurate (average relative error less than 1%) and computationally efficient (about 300 times faster than the physics-based model). After that, three optimal approaches were proposed to minimize the total energy consumption of the HTHP system. Approach 1 optimizes the load distribution between different heat pump units. Approach 2 optimizes the speed of fans and pumps by fixed approach and range of the condenser water (or evaporator solution). Approach 3 optimizes both the load distribution and the speed of fans and pumps. The optimization is implemented by using the ANN models, proposed approaches, and a genetic algorithm via a case study. The results show that the energy savings in the cooling season are 2.7%, 11.4%, and 14.8% by the three approaches, respectively. In the heating season, the energy savings of the three approaches are 1.6%, -1.4%, and 4.7%, respectively. Moreover, the thermodynamic performance in typical days was analyzed to investigate how energy savings could be achieved.

Key words: heating tower heat pump; model-based optimization; ANN model; genetic algorithm; energy saving

1. Introduction

Chillers with cooling towers are the most widely used systems for cooling supply in large commercial buildings due to their high energy efficiency [1]. Inspired by the heat rejection process in a standard cooling tower, previous research proposed a reversibly-used cooling tower, named as heating tower [2,3]. This tower can be used to transfer heat from ambient air to water or solution with low temperature. Due to the high demand of building heating supply in cool or cold regions, researchers proposed to replace the chillers with heat pumps and coupled them with the heating towers to fulfill the heating demand. The mean coefficient of performance (COP) of the heating tower heat pumps (HTHPs) in winter varied from 2.24 to 4.12 for different climate zones [4,5] And in summer, the HTHP could function as a water-cooled chiller with high efficiency [6]. The HTHP has shown significant advantages over the conventional heat pumps. For example, compared with the air-source heat pump (ASHP), the HTHP shows

higher efficiency and completely addresses the frosting problem. Comparing to the ground-source heat pump (GSHP), the HTHP has lower geographic limitation and lower initial cost. Therefore, the HTHP can be served as an alternative to the conventional heat pump for building cooling and heating in practical applications [7].

However, in previous research and applications of the HTHP [4,7], all components of the HTHP were running with constant speeds or fixed set points, which can be inefficient under varying weather conditions and building loads. Currently, few research has addressed the optimal operation of the HTHP system. Researches in optimal operation of water-cooled chiller systems can be used as a reference because these two systems have similarities in summer. For the optimization of the chiller plants, the near-optimal control and model-based optimal control were mainly investigated. The near-optimal control developed by Yu et al. [8], adopted simple polynomials to realize direct or indirect control of fan speed and pump speed. The wet-bulb temperature and part load ratio (PLR) of chillers were taken as the input variables in the polynomials. Those methods are simple and fast, which can be easily applied in the chiller plants with limited computational resources. However, achieving the energy savings cannot be guaranteed due to the simplification in system modeling. To improve the accuracy, Huang et al. [9] employed a Bayesian network model trained by optimal control setpoints computed by optimization algorithm with a high-fidelity physic model. The results showed that the energy saving ratio was improved by about 5.1% compared with the polynomial prediction, but still 0.2% lower than the model-based optimization method. Another problem in the near optimization is that the PLR of the chiller is calculated by a fixed maximum cooling capacity, instead of the actual capacity which is changing with the operating conditions. As a result, the optimal number of operating chillers determined by this method may be inappropriate.

To achieve the highest energy saving ratio, many researchers performed model-based optimizations for chiller plants. Three key steps of the model-based optimization are model development, control strategy selection, and optimization algorithm implementation. The following part will discuss each step in detail.

For the model development, regression models, physics-based models, and data-driven models are mostly used. The regression models are the fastest in computing speed, which then require much fewer computing efforts in model-based optimization [10,11]. However, they are reliable only for operating conditions within the range of the regression data, and extrapolation outside this range may lead to significant errors. In addition, all the existing regression models for chiller plants cannot be used to predict the performance of the HTHP system because they have different physical processes in winter. The physics-based models have no such limitations in analyzing the performance of the HTHP system, since the components models, system configuration, and operation mode can be changed by employing physical laws [12,13]. Although the physics-based models are effective, they always require high computational costs. When combined with global optimization techniques to seek the optimal solutions, the slow computing speed can prevent their online applications. To address this problem, data-driven models are proposed and adopted, which can achieve both fast computing speed and high accuracy [14,15]. However, it requires a vast amount of operational data to train the data-driven models. This is even more difficult for the newly sized or

installed the HTHP systems. In this paper, to address the above mentioned issues, we developed a physics-based model and validated it with a small amount of experimental data. Then, this new physics-based model was run under different combinations of weather and operation conditions to generate a vast amount of operational data for the data-driven models (artificial neural network models).

For the control strategy selection, the optimal load distribution and optimal fan and pump speeds were mainly discussed in the previous studies. Those two approaches were combined in some studies to achieve the highest possible energy saving ratio. The optimal load distribution method works because the chiller's COPs varies with its PLRs [16]. On one side, chillers, whose PLRs are adjusted by inlet guide vanes or modulating sliding valves, have the highest COP at full load due to the lower mechanical loss [17]. On the other side, chillers, whose PLR are adjusted by variable frequency drive (VFD), perform better at low PLRs than high PLRs due to the higher thermal heat exchange efficiency at low PLR [17]. The optimal load distribution method can still work when the chillers are replaced by heat pumps in the HTHP systems since the heat pump's COP is also a function of its PLR. In the optimal fan and pump speeds method, various indirect control variables (e.g. condenser water range, cooling tower approach, and condenser water supply temperature) are adopted to adjust the fan and pump speeds. Reducing the fan and pump speed at low PLRs can significantly reduce their energy consumption with little negative effects on the performance of chillers since the heat rejection capacity of the cooling tower is redundant at low PLRs. In the HTHP system, the heat rejection capacity of the tower in summer was about 3-4 times of its heat absorption capacity in winter [18]. Thus, the heating tower are sized to satisfy the heat absorption in winter. As a result, it has more redundant heat rejection capacity than the conventional cooling towers, which indicates that the heating tower has higher energy saving potential than conventional cooling towers. In winter, the energy use of the solution regeneration is an additional factor, which can significantly impact the optimization results.

For the optimization algorithm, the gradient-based algorithm was often adopted, including reduced gradient search, Hooke–Jeeves search, and Lagrangian method [10,11]. These methods are fast in convergence, but they can be trapped into local optima and require the gradient of objective function. Due to these limitations, they are often used in simple regression and need to couple with starting point selecting methods. The heuristic algorithms, such as genetic algorithm (GA), simulated annealing, and particle swarm optimization, were more popular in the optimization of chiller plants because they do not require the gradient of objective function [19,20]. Since the optimization of HTHP is a multi-variable, non-differentiable optimization problem, this study selects the GA which is a popular heuristic algorithm successfully used for the optimization of chiller plants.

In this paper, we described an existing HTHP and developed the physics-based model for it. Then, the artificial neural network (ANN) models were developed and trained with vast amount of operational data generated by the physics-based model. After that, the optimization problem, optimal approaches, and optimization algorithm were introduced. Using the GA and ANN models, the model-based optimization was conducted in a case study. Finally,

the annual energy savings of the proposed approaches were presented. Moreover, the thermodynamic performance of typical days was analyzed to investigate how energy savings could be achieved.

2. Modeling of the HTHP system

2.1. System description

Fig. 1 shows the schematics of a typical HTHP system in summer and winter conditions, respectively. This HTHP system consists of three identical HTHPs, which are practical HTHPs. Each HTHP has one heat pump, one heating tower, one tower side pump, and one user side pump. All equipment is dedicated to that HTHP. To investigate the energy-saving potential of different optimal approaches, this study adopted variable frequency drives for the compressors, tower fans, and tower side pumps.

In the summer condition, the HTHP runs as a water chiller with cooling tower. The condenser of the heat pump is connected with the heating tower which is used as cooling tower in summer with water as the working fluid. Heat rejection of the heat pump is done by the water evaporation in the tower, and the mass balance in this process is achieved by adding make-up water to the loop. The evaporator is connected with the building system to provide chilled water for the buildings.

In the winter condition, the connection between components is switched by external valves. Opposite to the summer condition, the evaporator is connected with the heating tower in winter, and water is replaced by solution with low freezing point (e.g. glycol aqueous) to avoid system freeze. The solution absorbs both sensible and latent heat from the atmosphere, and provides heat to the heat pump. Since the solution can be diluted in this process, a solution regeneration system based on vacuum boiling and condensation is equipped to achieve mass balance in this study. The details of the regeneration system can be found in our previous studies. This regeneration device is independent from the HTHP system, and the power used by it is to satisfy the gasification latent heat of water. Therefore, the regeneration device power has no influence on the heating capacity of the HTHP system[21,22].

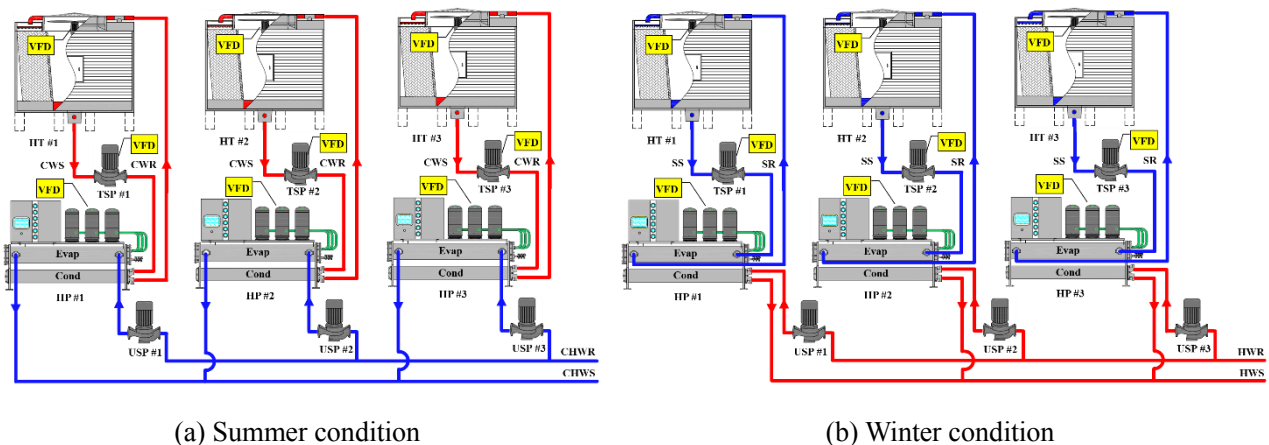(a) Summer condition   (b) Winter condition

Fig. 1. The schematic of the HTHP system (HT, heating tower; HP, heat pump; TSP, tower side pump; USP, user side pump; CWS/CWR, supply/return condenser water; CHWS/CHWR, supply/return chilled water; SS/SR, supply/return solution; HWS/HWR, supply/return hot water; VFD, variable frequency drive.)

2.2. System performance indexes

For the heating tower, the heat and mass transfer capacities are adopted:

$$Q_s = (Cp_a + \omega_a Cp_v) \cdot M_a \cdot (T_{a,o} - T_{a,i}) , \tag{1}$$

$$Q_l = r_v \cdot M_a \cdot (\omega_{a,o} - \omega_{a,i}) , \tag{2}$$

where Q_s is the sensible heat transfer capacity, and Q_l is the latent heat transfer capacity. Here, the positive values of Q_s and Q_l mean that the heat and mass transfer directions are from air to condenser water or solution. When the values are negative, the directions are the opposite. The Cp, M, T, ω, and r represent the specific heat, mass flow rate, temperature, humidity ratio, and vaporization latent heat, respectively. The subscripts a, v, i, and o represent the air, water vapor, tower inlet, and tower outlet, respectively.

Besides, the approach, τ, and range, ΔT, which are commonly used in the conventional cooling towers, are employed. For the winter condition, the wet-bulb temperature, T_{wb}, is replaced by the equivalent wet-bulb temperature, $T_{wb,eq}$, at which the equivalent enthalpy of solution is equal to the enthalpy of the ambient air [4].

$$\tau = \begin{cases} T_{cws} - T_{wb} , & \text{summer condition} \\ T_{wb,eq} - T_{ss} , & \text{winter condition} \end{cases} , \tag{3}$$

$$\Delta T = \begin{cases} T_{cwr} - T_{cws} , & \text{summer condition} \\ T_{ss} - T_{sr} , & \text{winter condition} \end{cases} . \tag{4}$$

The energy performance of the heat pump is measured by the coefficient of performance, COP:

$$COP = \begin{cases} \dfrac{Cp_w M_w (T_{chwr} - T_{chws})}{W_{HP}} , & \text{summer condition} \\ \dfrac{Cp_w M_w (T_{hws} - T_{hwr})}{W_{HP}} , & \text{winter condition} \end{cases} , \tag{5}$$

where subscript w represents the water. The W_{HP} is the power consumption of the heat pump.

The energy performance of the HTHP system is indicated by energy efficiency ratio, EER:

$$EER = \begin{cases} \dfrac{Cp_w M_w (T_{chwr} - T_{chws})}{W_{HP} + W_{TSP} + W_{HT}} , & \text{summer condition} \\ \dfrac{Cp_w M_w (T_{hws} - T_{hwr})}{W_{HP} + W_{TSP} + W_{HT} + W_{RD}} , & \text{winter condition} \end{cases} , \tag{6}$$

where W_{TSP}, W_{HT}, and W_{RD} are the power consumption of the tower side pump, fan, and regeneration device, respectively.

2.3. Physics-based model

The physics-based models of all equipment of the studied HTHP system were developed separately, and then coupled together using energy and mass balances between different equipment. The following sections describe the models for heat pump, heating tower, fan and pumps.

2.3.1. Heat pump model

The heat pump consists of four main components, including the scroll compressors, shell-tube evaporator, shell-tube condenser, and thermostatic expansion valve. Models of the components are developed as follows.

Compressor

The refrigerant mass flow rate, M_R, and power consumption, W_{comp}, for fixed speed scroll compressors can be expressed by a function of the evaporating temperature, T_e, and condensing temperature, T_c [23].

$$M_{R,rated} = \pi_1 + \pi_2 T_e + \pi_3 T_c + \pi_4 T_e^2 + \pi_5 T_e T_c + \pi_6 T_c^2 + \pi_7 T_e^3 + \pi_8 T_e^2 T_c + \pi_9 T_e T_c^2 + \pi_{10} T_c^3, \tag{7}$$

$$W_{comp,rated} = \pi_1 + \pi_2 T_e + \pi_3 T_c + \pi_4 T_e^2 + \pi_5 T_e T_c + \pi_6 T_c^2 + \pi_7 T_e^3 + \pi_8 T_e^2 T_c + \pi_9 T_e T_c^2 + \pi_{10} T_c^3, \tag{8}$$

where the subscript $rated$ represents the performance under rated speed. The regression coefficients are listed in Table 1.

Table 1. Regression coefficients of Eqs. (1) and (2)

Regression coefficients of Eq. (1)		Regression coefficients of Eq. (2)	
π_1	2.696×10^2	π_1	4.505
π_2	8.461	π_2	3.547×10^{-2}
π_3	-1.881	π_3	1.107×10^{-1}
π_4	1.261×10^{-1}	π_4	5.832×10^{-6}
π_5	-3.693×10^{-2}	π_5	8.214×10^{-5}
π_6	5.741×10^{-2}	π_6	-2.706×10^{-4}
π_7	1.154×10^{-3}	π_7	-8.487×10^{-7}
π_8	-1.006×10^{-3}	π_8	1.705×10^{-6}
π_9	9.011×10^{-4}	π_9	-9.203×10^{-6}
π_{10}	-7.020×10^{-4}	π_{10}	2.340×10^{-5}

For variable speed scroll compressors, M_R and W_{comp} were found proportional to the rotation speed, N_{comp} [24]. The above models with speed ratio correction can be used to express the performance of the variable speed scroll compressors [25]:

$$M_R = M_{R,rated} \frac{N_{comp}}{N_{comp,rated}} \,, \tag{9}$$

$$W_{comp} = W_{comp,rated} \frac{N_{comp}}{N_{comp,rated}} \,. \tag{10}$$

Evaporator and condenser

The classical logarithmic mean temperature difference method is adopted in both evaporator and condenser models. The cooling capacity of the evaporator, Q_e, and the heating capacity of the condenser, Q_c, can be expressed as follows:

$$Q_e = K_e A_e LMTD_e \,, \tag{11}$$

$$Q_c = K_c A_c LMTD_c \,, \tag{12}$$

where K, A, and $LMTD$ are the heat transfer coefficient, heat transfer area, and logarithmic mean temperature difference between refrigerant and water/ solution. The subscript e represents the evaporator, and c represents the condenser.

For the shell-tube evaporator, the refrigerant evaporates inside the tube, and the water/solution flows across the tube. The heat transfer coefficient for the evaporation of R22 inside the tube, K_R, can be described as follows:

$$K_R = (0.023 Re_{R,l}^{0.8} Pr_{R,l}^{0.4} \frac{\lambda_{R,l}}{d_i}) \cdot [c_1(c_0)^{c_2} \left(\frac{25G_R^2}{9.8\rho_{R,l}^2 d_i}\right)^{c_5} + 2.2c_3 \left(\frac{q_{R,i}}{G_R r_R}\right)^{c_4}] \quad , \tag{13}$$

$$c_0 = \left(\frac{1-x}{x}\right)^{0.8} \left(\frac{\rho_{R,g}}{\rho_{R,l}}\right)^{0.5} \quad , \tag{14}$$

where Re is the Reynolds number, and Pr is the Prandtl number. The λ, G, ρ, q, and x are the thermal conductivity coefficient, mass flow flux, density, inner heat flux, and dryness, respectively. The subscript R is the refrigerant. The subscript l and g represent the liquid phase and gas phase, respectively. The d_i is the inner diameter of the tube. The c_0 is the characteristic number of convection heat transfer, and c_1-c_5 are constants depending on c_0. The heat transfer coefficient of the water/solution across the tube, K_w (or K_s), can be expressed as follow:

$$K_w = 0.22 Re_w^{0.6} Pr_w^{1/3} \frac{\lambda_w}{d_0} \quad , \tag{15}$$

$$K_s = 0.22 Re_s^{0.6} Pr_s^{1/3} \frac{\lambda_s}{d_0} \quad , \tag{16}$$

where the subscript s represents the solution. The d_o is the external diameter of the tube.

For the shell-tube condenser, the refrigerant condenses outside the tube, and the water flows inside the tube. The heat transfer coefficient for the condensation of R22 outside the tube, K_R, and the heat transfer coefficient of the water flowing inside the tube, K_w, are shown as follows:

$$K_R = 0.725 \left(\frac{9.8\lambda_{R,l}^3 \rho_{R,l}^2 r_R}{u_{R,l}}\right)^{0.25} d_o^{-0.25} (T_c - T_{wall})^{-0.25} \Psi_1 \varepsilon_1 \quad , \tag{17}$$

$$K_w = 0.023 Re_w^{0.8} Pr_w^{0.4} \frac{\lambda_w}{d_i} \quad , \tag{18}$$

where $u_{R,l}$ is liquid phase dynamic viscosity of the refrigerant, and T_{wall} is the temperature of the tube wall. The Ψ_1 and ε_1 are correction factors depending on the size and arrangement of tubes.

Based on the coefficients of refrigerant, water and solution for different processes, the overall heat transfer coefficient for the evaporator or condenser, K_e (K_c), can be expressed as a function of the heat transfer coefficient inside the tube, K_i, and outside the tube, K_o:

$$K_e \ (K_c) = \frac{1}{\left(\frac{1}{K_i}+R_i\right)\frac{A_o}{A_i}+\frac{\delta A_o}{\lambda_{wall}A_m}+R_o+\frac{1}{K_o}} \quad , \tag{19}$$

where R is the heat transfer resistance. The δ is the thickness of the wall. The subscripts i and o represent the property inside and outside the tube, respectively. And the subscripts m is the mean value of the inside and outside property.

The heat transfer capacities of the evaporator and condenser can be expressed by the energy variations of refrigerant and water/solution.

$$Q_e = M_R(h_1 - h_4) \quad , \tag{20}$$

$$Q_e = M_w Cp_w (T_{chwr} - T_{chws}) \quad \text{or} \quad Q_e = M_s Cp_s (T_{ss} - T_{sr}) \ , \tag{21}$$

$$Q_c = M_R (h_2 - h_3) \ , \tag{22}$$

$$Q_c = M_w Cp_w (T_{cwr} - T_{cws}) \ or \ Q_c = M_w Cp_w (T_{hws} - T_{hwr}) \ , \tag{23}$$

where h_1 and h_4 are the enthalpy of the refrigerant in the inlet and outlet of the evaporator, h_2 and h_3 are the enthalpy of the refrigerant in the inlet and outlet of the condenser.

Expansion valve

The expansion process in the expansion valve is taken as an isenthalpic process as shown in Eq.(24). The mass flow rate of the refrigerant can be calculated by Eq. (25) [26].

$$h_3 = h_4 \ , \tag{24}$$

$$M_R = C_D A_{th} \sqrt{\rho_{R,l} (P_c - P_e)} \quad , \tag{25}$$

where, C_D is the constant mass flow coefficient. The A_{th} represents the geometric throat area of the thermostatic expansion, which is adjustable and controlled by the superheat. The P_c and P_e are the pressure of condenser and evaporator, respectively.

2.3.2. Heating tower model

The model of the heating tower in winter is developed using a finite difference method [3]. Eqs.(26) and (27) express the energy and mass balances between air and solution. Eq.(28) describes the solute balance of the solution.

$$m_a dh_a = -Cp_s m_s dT_s - Cp_s T_s dm_s \ , \tag{26}$$

$$dm_s = -m_a d\omega_a \ , \tag{27}$$

$$X_s m_s = (X_s + dX_s)(m_s + dm_s) \ , \tag{28}$$

where dh_a is the enthalpy variation of the air through an element. The dT_s, dm_s and dX_s represent the variations of the solution in temperature, mass flow rate and concentration through an element, respectively. The X_s is the mass concentration of the solution.

The convective heat and mass transfer are also applied as shown in Eqs.

$$h_c L \cdot dx \cdot dy \cdot \alpha_w (T_s - T_a) = m_a (Cp_a + \omega_a Cp_v) dT_a \ , \tag{29}$$

$$h_d L \cdot dx \cdot dy \cdot \alpha_w (\omega_s - \omega_a) = m_a d\omega_a \ , \tag{30}$$

where ω_s is the equivalent humidity ratio of the solution, dT_a and $d\omega_a$ are the temperature and humidity ratio variation of air through an element. The $dx \cdot dy$ represents the size of each element, L is the length of the packing, and α_w is the specific area of the packing. The h_c is the heat transfer coefficient, h_d is the mass transfer coefficient. These two coefficients are expressed as functions of the solution mass flow flux, G_s, and air mass flow flux, G_a, using iteration method and data from a practical heating tower [3].

$$h_c = \pi_1 G_s^{\pi_2} G_a^{\pi_3} \ , \tag{31}$$

$$h_d = \pi_1 G_s^{\pi_2} G_a^{\pi_3} \ . \tag{32}$$

By replacing the subscript s with w and setting X_s to zero, the model listed above can also be used to simulate the performance in summer.

2.3.3. Pump and fan model

The characteristic curves of pump and fan are often provided by manufacturers, while the characteristic curves of pipeline are difficult to know in the practice. Therefore, it is hard to determine the power consumption of pump and fan, which is calculated by the equipment characteristic curve and the pipeline characteristic curve. In this study, regression models were adopted to calculate the performance of fan and pump.

$$W_{TSP} = \pi_1 + \pi_2 \left(\frac{N_{TSP}}{N_{TSP,rated}} \right) - \pi_3 \left(\frac{N_{TSP}}{N_{TSP,rated}} \right)^2 + \pi_4 \left(\frac{N_{TSP}}{N_{TSP,rated}} \right)^3 \ , \tag{33}$$

$$W_{HT} = \pi_1 - \pi_2 (\frac{N_{HT}}{N_{HT,rated}}) + \pi_3 \left(\frac{N_{HT}}{N_{HT,rated}} \right)^2 + \pi_4 \left(\frac{N_{HT}}{N_{fan,rated}} \right)^3 \ . \tag{34}$$

And the data in our previous study was adopted to fit the coefficients of the above equations [4]. The results are listed in Table 2.

Table 2. Coefficients of Eqs. (33) and (34)

Regression coefficient	π_1	π_2	π_3	π_4
Eq. (33)	1.761×10^{-4}	8.264×10^{-1}	-7.857×10^{-1}	3.707
Eq. (34)	3.088×10^{-4}	-1.558×10^{-1}	3.852	2.483×10^{-1}

2.4 Data-driven model

The physics-based model adopting physical laws has high accuracy. However, it is time consuming and needs a lot of computing resources, since it contains several iterations and a great number of grids for the finite difference scheme applied on the heating tower model. This study used a Lenovo T450 computer with a four-core processor (I5-5200U, 2.2 GHz). The physics-based model developed in this study takes about 41.4 s to simulate one working condition in summer (cooling mode), and 101.7 s for one working condition in winter (heating mode). This is unacceptable in the model-based optimization since we need to run hundreds of simulations to identify the control settings for one working condition, and it takes several hours. Therefore, it is helpful to replace the complex physical models for the heat pump and heating tower by fast computing models. We still use the models for pump and fan as they are simple and easy to compute. The ANN models were selected due to its high accuracy and fast computing.

2.4.1. ANN model development

To develop the ANN models, we first define the dependent and independent variables for each equipment. For the heat pump model in summer, as shown in Fig. 2 (a), five independent variables are identified, including the speed of the compressor (N_{comp}), speed of tower side pump ($N_{pump} \ or \ M_{cw}$), speed of the user side pump ($N_{pump} \ or \ M_{chw}$), condenser water supply temperature (T_{cws}), and chilled water supply temperature (T_{chws}). There are two dependent variables, such as the coefficient of performance (COP) and cooling capacity of the heat pump

(Q_e). The other parameters (e.g. the condenser water return temperature, chilled water return temperature, and capacity of the condenser) can be calculated by the independent and dependent variables. Therefore, the input matrix can be expressed as $[N_{comp}, M_{cw}, M_{chw}, T_{cws}, T_{chws}]$, and the output matrix is $[COP, Q_e]$. In winter, besides the five independent variables mentioned above, the concentration of the solution (X_s) should also be added as an independent variable. Thus, the inputs and outputs can be expressed as $[N_{comp}, M_{hw}, M_s, T_{hws}, T_{ss}, X_s]$ and $[COP, Q_c]$.

For the heating tower model in summer, independent variables are identified as the outdoor air dry-bulb (T_{db}), wet-bulb temperature (T_{wb}), speed of the tower fan (N_{fan} or M_a), mass flow rate of the condenser water (M_{cw}), and condenser water return temperature (T_{cwr}). The sensible heat transfer capacity (Q_s) and latent heat transfer capacity (Q_l) of the tower are the dependent variables. Therefore, the inputs and outputs of the tower model can be expressed as $[T_{db}, T_{wb}, M_a, M_{cw}, T_{cwr}]$ and $[Q_s, Q_l]$, respectively. Similarly, the inputs and outputs of the tower model in winter are $[T_{db}, T_{wb}, M_a, M_s, T_{sr}, X_s]$ and $[Q_s, Q_l]$. Different from the conventional cooling tower model which only takes the T_{wb} as input weather data, the T_{db} is also considered here, since both heat and mass transfer cannot be ignored in the heating tower.

According to recommended numbers of the nodes and hidden layers [27], a back-propagation (BP) network with two hidden layers and ten nodes in each hidden layer was employed. The BP network was implemented under the MATLAB environment. We tried several commonly used activation functions (e.g. Sigmold, tanh, ReLu), and selected the functions by assessing the calculation accuracy and time of the ANNs. The Tansig function was adopted as the transfer function between the first three layers, and Purelin function served the last two layers, respectively. The structures of the BP networks adopted for the four models are presented in Fig. 2.
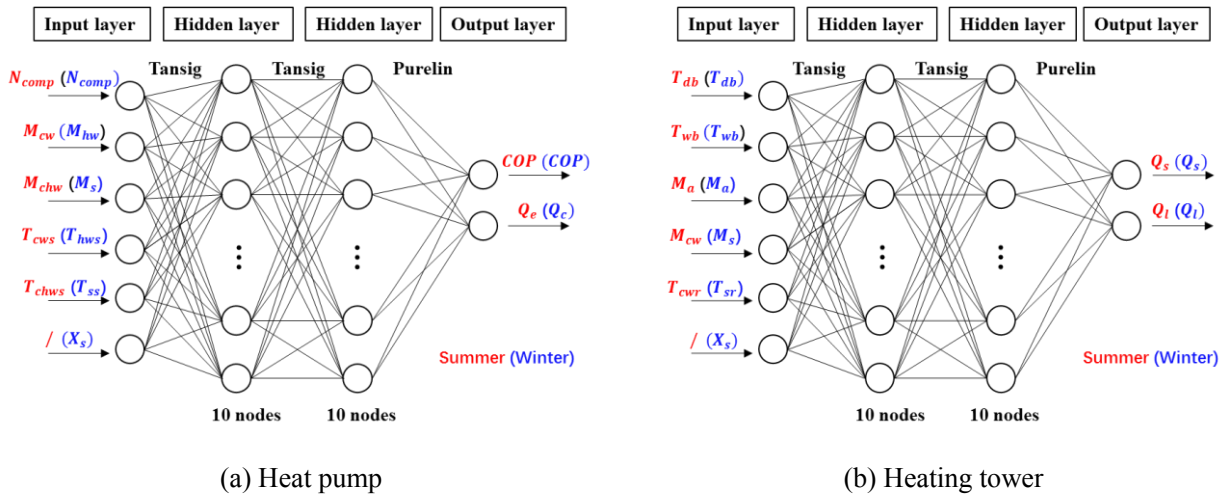

(a) Heat pump　　　　　　　　　　　　　　　(b) Heating tower

Fig. 2. The structure of the BP network for modeling

2.4.2. Model training and validation

For each ANN model, 18,000 data sets were used for training, the rest 2,000 data sets were adopted for validation. In order to improve the prediction agreement, all the data were normalized into the range of -1 to 1. The

Levenberg-Marquardt acted as the training function, and the mean squared error was used as the performance index, during the training process. This section introduces the generation of training and validation data, and the results are shown in Section 4.2.

20,000 input data sets for heat pump model in summer were generated randomly in the following ranges: $N_{comp} \in [580, 2900]$ Rev. min^{-1}, $M_{cw} \in [18.5, 37]$ m^3 h^{-1}, $M_{chw} \in [11, 22]$ m^3 h^{-1}, $T_{cws} \in [15, 35]°C$, $T_{chws} \in [7, 9]°C$. Similarly, the ranges of the 20,000 input data sets for heat pump model in winter are $N_{comp} \in [580,2900]$ Rev. min^{-1}, $M_{hw} \in [11,22]$ m^3 h^{-1}, $M_s \in [18.5,37]$ m^3 h^{-1}, $T_{hws} \in [44,46]°C$, $T_{ss} \in [-12,15]°C$, and $X_s \in [0,0.4]$. After the generation of each X_s, the freezing point of the solution will be verified to make sure it is lower than the solution temperature. For the heating tower model in summer, the ranges of the 20,000 data sets are $T_{db} \in [15,38]°C$, $M_a \in [4300,43000]$ m^3 h^{-1}, $M_{cw} \in [18.5,37]$ m^3 h^{-1}, $T_{cwr} \in [20,40]°C$. For the heating tower model in winter, the ranges of the 20,000 data sets are $T_{db} \in [-6,20]°C$, $M_a \in [4300,43000]$ m^3 h^{-1}, $M_s \in [18.5,37]$ m^3 h^{-1}, $T_{sr} \in [-13,15]°C$, $X_s \in [0,0.4]$. Particularly, the T_{wb} is calculated by T_{db} and the relative humidity (φ_a) from 15% to 100%, to avoid physical violations. With the input data sets mentioned above, the corresponding outputs were computed by the physics-based model in both summer and winter conditions.

3. Model-based optimization of the HTHP system

3.1. Optimization formulation

The aim of the optimization work is to minimize the power consumption of the HTHP system with time-varying building load and weather data. For a typical HTHP system described in Section 2.1, the major energy consumers in summer are heat pumps, tower side pumps, and tower fans. In winter, besides the above three equipment, the energy consumption of the regeneration drive should be also counted. Thus, the objective functions can be expressed as:

$$J_{summer} = \min(\sum_{i=1}^{3} W_{HP,i} + \sum_{i=1}^{3} W_{TSP,i} + \sum_{i=1}^{3} W_{HT,i}) , \tag{35}$$

$$J_{winter} = \min(\sum_{i=1}^{3} W_{HT,i} + \sum_{i=1}^{3} W_{TSP,i} + \sum_{i=1}^{3} W_{HT,i} + W_{RD}) . \tag{36}$$

When the heat pump model, heating tower model and building system are coupled together, some interaction constraints need to be satisfied. The actual cooling/heating load provided by the system should be the same as the building load. In addition, the properties of the condenser water (or solution) entering and exiting the heat pump should be the same as those of the heating tower. Besides, the mechanical constraints provided by the manufacturers should be satisfied:

$$20\%N_{comp,rated} \leq N_{comp} \leq 100\%N_{comp,rated}, \tag{37}$$

$$50\%M_{cw,rated} \leq M_{cw} \leq 100\%M_{cw,rated}, \tag{38}$$

$$50\%M_{s,rated} \leq M_s \leq 100\%M_{s,rated}, \tag{39}$$

$$10\%M_{a,rated} \leq M_a \leq 100\%M_{a,rated}. \tag{40}$$

In addition, some constraints of the operation parameters should also be satisfied. In the summer condition, the T_{cws} should be higher than 15°C as required by the manufacturers to avoid the small pressure difference of the compressor. In the winter condition, the freezing point of the solution should be lower than the T_{sr}, which is the lowest temperature in the system, to prevent system from freeze. Here, the penalty function is adopted to address the constrained optimization problems. By introducing the penalty coefficients, K_p, the objective functions in Eqs.(35) and (36) can be converted into:

$$J_{summer} = \min(\sum_{i=1}^{3} W_{HP,i} + \sum_{i=1}^{3} W_{TSP,i} + \sum_{i=1}^{3} W_{HT,i} + K_{p1}\max(0, 15 - T_{cws})) \; , \tag{41}$$

$$J_{winter} = \min(\sum_{i=1}^{3} W_{HP,i} + \sum_{i=1}^{3} W_{TSP,i} + \sum_{i=1}^{3} W_{HT,i} + W_{RD} + K_{p2}\max(0, T_f - T_{sr})) \; , \tag{42}$$

where T_f is he freezing point of the solution. In this study, the T_{chws} in summer is set as 7°C, and the T_{hws} in winter is set as 45°C.

3.2. Conventional control strategy (baseline)

The conventional control strategy used in the practical HTHP systems is taken as the baseline of this study. The tower side pump and tower fan are kept at fixed speeds for both summer and winter conditions. The number and speed of the operating heat pumps are variables to meet the changing building load. Another heat pump will be brought on-line when the on-line heat pumps operating with full capacity cannot satisfy the building load. Thus, the objective functions can be expressed as follows.

$$J_{summer} = \min(f_1(Q_{load}, T_{db}, T_{wb}) + K_{p1}\max(0,15 - T_{cws})) \; , \tag{43}$$

$$J_{winter} = \min(f_2(Q_{load}, T_{db}, T_{wb}) + K_{p2}\max(0, T_f - T_{sr})) \; , \tag{44}$$

where Q_{load} is the building load.

3.3. Optimal approaches

Table 3 summarizes the configurations of the four different approaches including the baseline and three proposed optimal approaches. This section provides some detailed descriptions of the optimal approaches.

Table 3. Summary of the four approaches

Optimization approach	Heat pump	Heating tower fan and pump
Baseline	Sequential control	Fixed fan speed and pump speed
Approach 1	Optimal load distribution	Fixed fan speed and pump speed
Approach 2	Sequential control	Fixed approach and range (approach at 4°C, range at 5°C in summer; approach at 4°C, range at 3°C in winter)
Approach 3	Optimal load distribution	Optimal fan speed and pump speed

3.3.1. Approach 1: optimal load distribution

The focus of baseline is to minimize the amount of on-line equipment. This permits heat pumps to operate as close as possible to their full capacity. However, the heat pump with the VFD shows higher efficiency when it

operates well below full load. Because, the heat exchange areas of both the evaporator and condenser are redundant in part load, which reduces the $LMTD_e$ and $LMTD_c$. The purpose of approach 1 is to optimize the load distribution of the heat pumps to take advantage of the efficiency improvement in part load. Accordingly, the objective functions can be expressed as follows:

$$J_{summer} = \min(f_1(Q_{load}, T_{db}, T_{wb}, N_{HP,1}, N_{HP,2}, N_{HP,3}) + K_{p1}\max(0,15 - T_{cws})) \ , \tag{45}$$

$$J_{winter} = \min(f_2(Q_{load}, T_{db}, T_{wb}, N_{HP,1}, N_{HP,2}, N_{HP,3}) + K_{p2}\,max(0, T_f - T_{sr})) \ . \tag{46}$$

3.3.2. Approach 2: fixed approach and range

Approach 2 is widely used in the optimization of condenser water systems of chiller plants. When the building load is low in summer, the heat rejection capacity of the heating tower is redundant, while the T_{cws} is limited by the T_{wb}. As a result, the HTHP has only a little improvement in COP of the heat pump and consumes more energy with full speed fans. In addition, the temperature difference between return and supply condenser water (range), ΔT_{cw}, can be quite small with low cooling load, which indicates that the energy of the pumps can be saved in this condition. Approach 2 adjusts the M_a and M_{cw} to maintain a constant approach and range. According to the conventional cooling tower, the fixed approach and range are set as 4 °C and 5 °C, respectively. Similarly, the M_a is controlled by a fixed approach of 4 °C, and the M_s is controlled by a fixed range of 3 °C in winter. Accordingly, the objective functions can be expressed as follows.

$$J_{summer} = \min(f_1(Q_{load}, T_{db}, T_{wb}, \tau, \Delta T_{cw}) + K_{p1}\max(0,15 - T_{cws})) \ , \tag{47}$$

$$J_{winter} = \min(f_2(Q_{load}, T_{db}, T_{wb}, \tau, \Delta T_s) + K_{p2}\,max(0, T_f - T_{sr})) \ . \tag{48}$$

3.3.3. Approach 3: optimal all control variables

Approach 3 adopts the optimization technique, to find a set of setpoints for all the control variables, including N_{HP}, M_a, and M_{cw} (M_s), to achieve a minimum system energy consumption. Accordingly, the objective functions of this approach can be expressed as:

$$J_{summer} = \min(f_1(Q_{load}, T_{db}, T_{wb}, N_{HP,1}, N_{HP,2}, N_{HP,3}, M_{a,1}, M_{a,2}, M_{a,3}, M_{cw,1}, M_{cw,2}, M_{cw,3}) + \tag{49}$$
$$K_{p1}\max(0,15 - T_{cws})) \ ,$$

$$J_{winter} = \min(f_2(Q_{load}, T_{db}, T_{wb}, N_{HP,1}, N_{HP,2}, N_{HP,3}, M_{a,1}, M_{a,2}, M_{a,3}, M_{s,1}, M_{s,2}, M_{s,3}) + \tag{50}$$
$$K_{p2}\,max(0, T_f - T_{sr})) \ .$$

3.4. Optimization algorithm

The optimization problems described above are multi-variables, non-differentiable problems, which cannot be addressed by the commonly used gradient-based method. Here, the GA was implemented under the MATLAB environment to address the optimization problems.

4. Case study

4.1. Case description

To validate the proposed method, a case study of a four-story office building located in Nanjing, China, was carried out. The HTHP system serving the building has three identical heat pumps, three identical heating towers, three identical tower side pumps, and one regeneration device. The details of the building and HTHP system are presented in Table 4.

Table 4. Details of the building and HTHP system

Building			
Building type	Office	Location	Nanjing, China
Floor area	4,500 m^2	Schedule	8:00 — 18:00
Floors	4	Weather data	GB 50736-2012 [28]
Cooling season	May 15th — Sep. 30th	Heating season	Nov. 15th — Mar. 15th
Peak cooling load	422.0 kW	Peak heating load	345.0 kW
Annual cooling load	296,466 kWh	Annual cooling load	242,682 kWh
Heat pumps (one of the identical three)			
Compressor Type	Scroll		
Nominal cooling Q_e	132.6 kW	Nominal heating Q_c	116.6 kW
Nominal cooling W_{comp}	29.0 kW	Nominal heating W_{comp}	35.5 kW
Design cooling COP	4.6	Design heating COP	3.3
Design T_{chws} / T_{chwr}	7 / 12.2°C	Design T_{hws} / T_{hwr}	45.0 / 40.4°C
Design M_{chw}	22.0 m^{3}h^{-1}	Design M_{hw}	22.0 m^{3}h^{-1}
Design T_{cws} / T_{cwr}	29.3 / 33.1°C	Design T_{ss} / T_{sr}	0.2 / -1.8°C
Design M_{cw}	37.0 m^{3}h^{-1}	Design M_s	37.0 m^{3}h^{-1}
Heating towers (one of the identical three)			
Design air flow rate	43000 m^{3}h^{-1}	Fan power	3.9 kW
Summer design T_{db} / T_{wb}	32.0 / 28.0°C	Winter design T_{db} / T_{wb}	7.0 / 5.0°C
Summer design approach / range	1.3 / 3.8°C	Winter design approach / range	5.1 / 2.0°C
Tower side pump (one of the identical three)			
Rated power	3.7 kW	Rated flow rate	37.0 m^{3}h^{-1}
Regeneration device			
Regeneration efficiency	3.4 kg kWh^{-1}		

The PLR-COP curve of the heat pump mentioned above is presented in Fig. 3. The results were generated by using the heat pump model developed in this study and the model was validated against the experimental data shown in Section 4.2. In summer condition, the T_{cws} is set as 29.3°C, and the T_{chws} is fixed as 7.0°C. In winter condition, the T_{ss} and T_{hs} are 0.2°C and 45°C, respectively. As indicated in Section 3.3.1, the heat pump assisted with the VFD shows higher efficiency when it operates in lower PLR. This characteristic provides the energy saving potential for the optimal load distribution method (Approach 1).
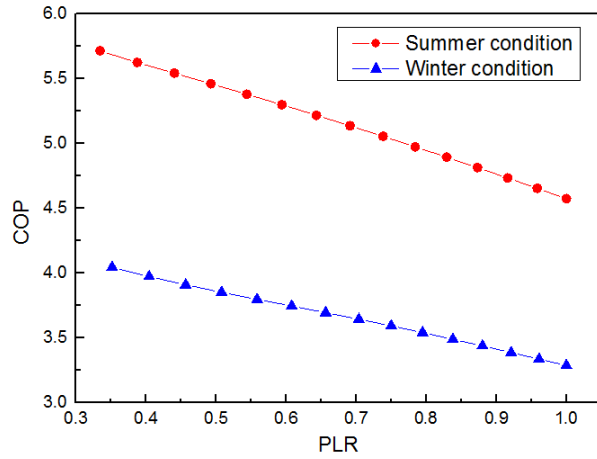
Fig. 3. PLR-COP curve of the heat pump

This case study adopts the hourly weather data of Nanjing from Chinese national standard GB 50736-2012 [28], as shown in Fig. 4. The corresponding building cooling and heating loads are calculated by the DEST simulation tools, and the results are demonstrated in Fig. 5.
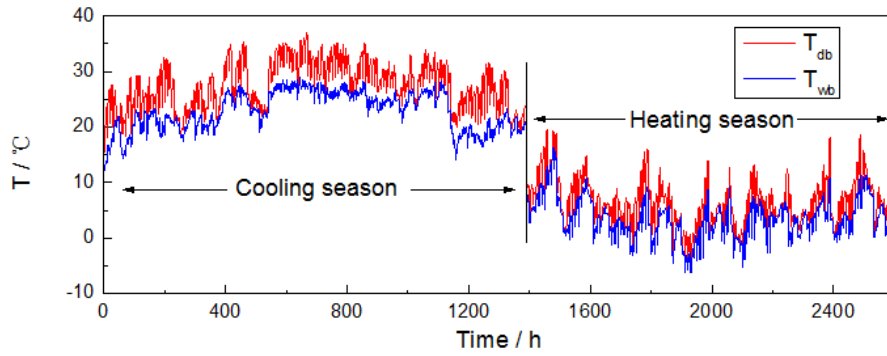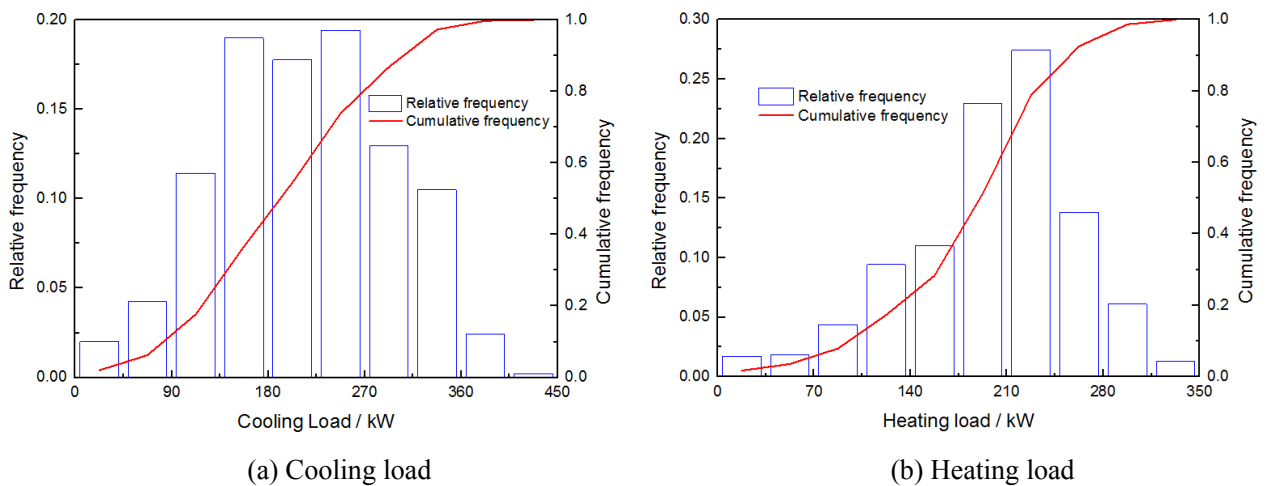

Fig. 4. Weather data

(a) Cooling load

(b) Heating load

Fig. 5. Building load distribution

4.2. Validation of the physics-based model and ANN model

For the physics-based model, the regression coefficients of Eqs.(7) and (8) are fitted using the data provided by the compressor manufacturers [29]. The coefficients of Eqs. (31), (32), (33), and (34) are regressed according to our experimental data [3,4]. Besides the operation parameters of the system listed in Section 4.1, the structure parameters are also important for the model development. All the above coefficients and parameters used in this study are presented in Table 5.

Table 5. Coefficients and structure parameters of the physics-based model

Components	Coefficients and parameters
Scroll compressor	π_{1-10} for Eq.(7): 2.696×10^2, 8.461, -1.881, 1.261×10^{-1}, -3.693×10^{-2}, 5.741×10^{-2}, 1.154×10^{-3}, -1.006×10^{-3}, 9.011×10^{-4}, -7.020×10^{-4} π_{1-10} for Eq.(8): 4.505, 3.547×10^{-2}, 1.107×10^{-1}, 5.832×10^{-6}, 8.214×10^{-5}, -2.706×10^{-4}, -8.487×10^{-7}, 1.705×10^{-6}, -9.203×10^{-6}, 2.340×10^{-5}
Shell-tube evaporator	Heat exchange area: 10.5 m^2 Tube side: R22, tube size Φ12.7×1.0, tube length 2000 mm, tube number 134, single flow, 15% copper-nickel alloy, internal thread Shell side: Water/solution, shell size Φ273×8, double flow, baffle thickness 50mm, baffle number 17
Shell-tube condenser	Heat exchange area: 7.2 m^2 Tube side: Water/solution, tube size Φ15.9×1.0, tube length 2000 mm, tube number 72, double flow, red copper, external reticulation Shell side: R22, Φ273×8, 2000 mm×1, single flow, division plate 28mm×2
Heating tower	Tower type: mechanical draft cross-flow PVC structured packings: length×width×height = 2×0.76×2 m (each side) Specific surface area: 172 m^2 m^{-3} π_{1-3} for Eqs.(31) and (32): 5.9040, 0.6035, 0.5906
Pump and fan	π_{1-4} for Eq.(33): 1.761×10^{-4}, 8.264×10^{-1}, 7.857×10^{-1}, 3.707 π_{1-4} for Eq.(34): 3.088×10^{-4}, 1.558×10^{-1}, 3.852, 2.483×10^{-1}

The physics-based model developed in this study is validated using our experimental data [4], as shown in Fig. 6. The relative error is within ±10% for all the predicted values, and the average error is 3.48% for cooling/heating capacity, and 3.05% for the COP. This indicates that the physics-based model has high accuracy in predicting the performance of the HTHP.

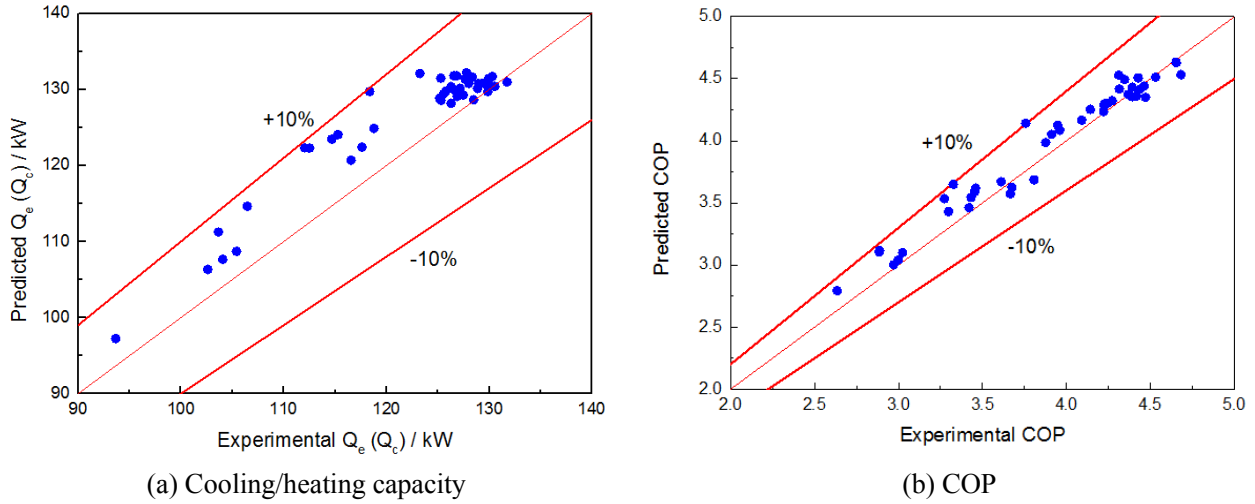| (a) Cooling/heating capacity | (b) COP |

Fig. 6. Comparison between the experimental data and the model prediction of the HTHP

The performance predicted by the ANN model is compared with that calculated by the validated physics-based model. As shown in Fig. 7, 2,000 data sets are used for the validation of the ANN models. The average relative error of $Q_e(Q_c)$ is 0.82%, and that of COP is 0.78%. Since the input data sets are generated randomly, the cooling/heating capacities can be small in some conditions (e.g. the combination of low compressor, fan, and pump speeds). In such situations, the relative errors can be up to 10%, but the absolute errors are still small. The root-mean-square error (RMSE) is also employed here. The RMSE of $Q_e(Q_c)$ is 0.99 kW when $Q_e(Q_c)$ varies from 15 to 175 kW. And the RMSE of COP is 0.07 when COP varies from 2.0 to 9.5. This indicates that the ANN models can accurately reflect the influence of the input parameters on the performance indexes. In addition, the mean computation time for one working condition in summer reduces from 41.4 s to 0.23 s, and that in winter condition reduces from 101.7 s to 0.25 s. This makes the model-based optimization viable in the practice.
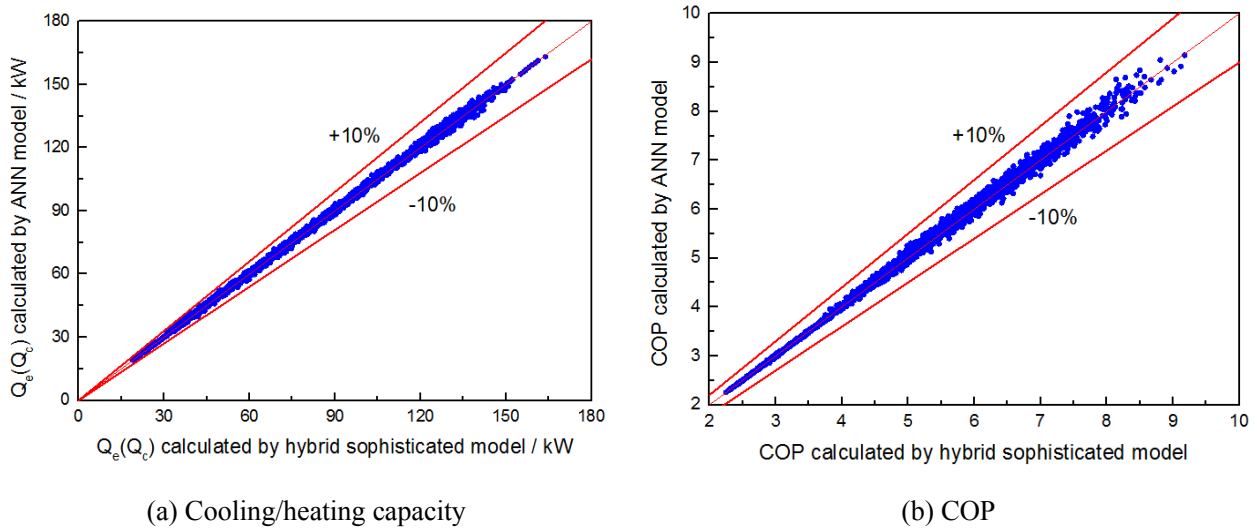

| (a) Cooling/heating capacity | (b) COP |

Fig. 7. Comparison between the performance of heat pump calculated by physics-based model and ANN model

4.3. Validation of the genetic algorithm

Based on the ANN models, the optimization objective functions of the proposed approaches can be calculated accurately and quickly. Then the GA was employed to find the global minimum of the objective functions. In this paper, the settings of GA are set up as follows: the population size is 30, the generation number is 20, the crossover probability is 0.6, and the migration probability is 0.01. Here, the results of the exhaustive search are taken as the baseline, in which we calculate the $1/EER$ with the variables (N_{comp}, M_{cw}/M_s, M_a) varying from the minimum to the maximum as indicated in Eqs.(37)-(40). The optimization result of $1/EER$ in a typical summer condition is presented in Fig. 8 (a). The baseline value is 0.273 under this condition. And the optimization result of $1/EER$ is shown as Fig. 8 (b) and its baseline value is 0.482. The results show that the GA can find the global optimum within 20 generations.

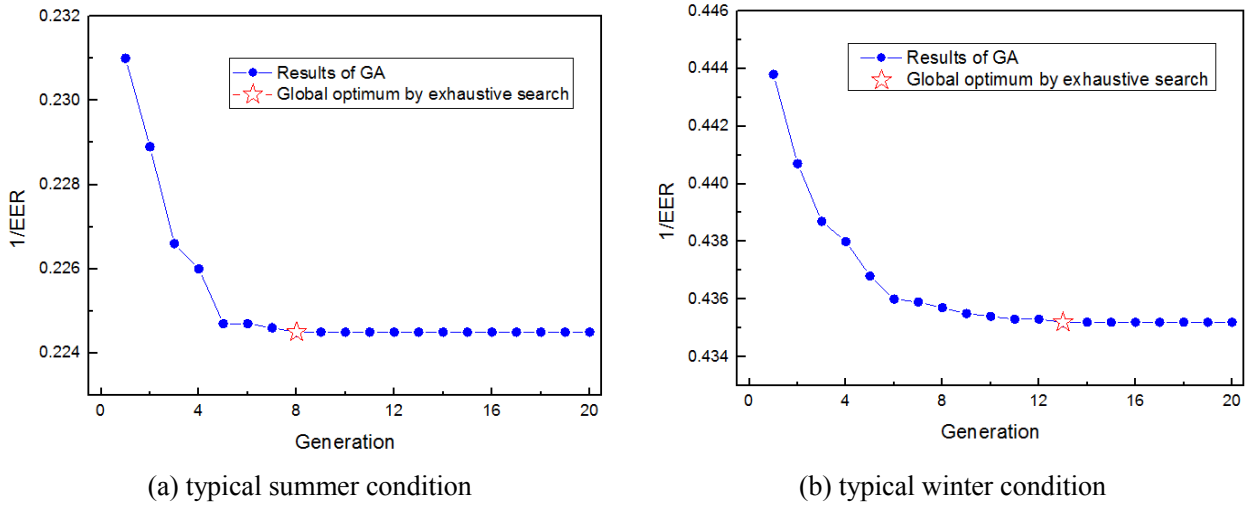(a) typical summer condition   (b) typical winter condition

Fig. 8. Validation of the genetic algorithm

4.4. Results and discussion

4.4.1. Annual energy saving performance analysis

Table 6 demonstrates the energy savings of different approaches compared with the baseline in the cooling season. The baseline consumes 77,889 kWh energy, of which the energy consumptions of the heat pumps, tower side pumps, and tower fans account for 73.0%, 13.1%, and 13.9%, respectively. Approach 1 can reduce the total energy consumption by 2.7%. This is mainly due to the efficiency improvement of the heat pumps in part load as presented in Fig. 3, while the energy consumptions of fans and pumps are the same as the baseline. Approach 2 increases the energy saving ratio to 11.4% by controlling the air and condenser water flow rates with fixed approach and range. In this approach, the fans and pumps operate with variable speed instead of fixed full speed. As a result, the energy saving ratios of pumps and fans are as high as 62.8% and 81.6%. However, the energy use of the heat pumps increases by 11.4% due to the rise of the condenser water supply temperature. As expected, Approach 3

shows the highest energy saving ratio by optimizing all the control variables. The energy saving ratios of different components are presented (68.4% and 74.3% savings for pumps and fans, 6.1% more energy use for heat pumps).

Table 6. Energy saving performance in cooling season

Approach	Baseline	Approach 1		Approach 2		Approach 3	
Energy consumption and saving ratio	kWh	kWh	/	kWh	/	kWh	/
Total	77,889	75,800	2.7%	68,994	11.4%	66,337	**14.8%**
Heat pump	56,882	54,793	3.7%	63,224	-11.1%	60,346	-6.1%
Tower side pump	10,166	10,166	0.0%	3,779	62.8%	3,209	68.4%
Tower fan	10,841	10,841	0.0%	1,991	81.6%	2,781	74.3%

Table 7 presents the energy saving performance of all the approaches in the heating season. The baseline consumes 94,265 kWh energy, of which the energy consumptions of the heat pumps, tower side pumps, and tower fans account for 77.2%, 10.0%, and 10.7%, respectively. In addition, the regeneration device only uses 2.1% of the total energy consumption. This is because the heating tower can run into self-regeneration process when the outdoor temperature is high and humidity ratio is low [30], and the high air and solution flow rates in the baseline enhances this process. In Approach 1, 1.6% energy saving ratio is achieved by optimizing the load distribution of the heat pumps, due to the 3.2% improvement of the heat pumps. Different from the results in the cooling season, Approach 2 costs even more energy (1.4%) than the baseline in the heating season. Since the fixed approach and range allow much lower air and solution flow rates, it shows big energy saving ratios for pumps and fans (77.5% and 52.5%). However, the energy used by the regeneration device is about 5.5 times of that in the baseline, because the self-regeneration processes are significantly weakened. Approach 3 has the highest energy saving ratio of 4.7%. The energy consumption of pumps and fans are reduced by 55.3% and 29.9%, respectively. And the energy use of the heat pumps has a slightly increase of 2.7% because of the reduction of solution supply temperature. Due to the same reason as Approach 2, the energy use of the regeneration device is doubled.

Table 7. Energy saving performance in heating season

Approach	Baseline	Approach 1		Approach 2		Approach 3	
Energy consumption and saving ratio	kWh	kWh	/	kWh	/	kWh	/
Total	94,265	92,772	1.6%	95,580	-1.4%	89,822	**4.7%**
Heat pump	72,780	70,449	3.2%	78,162	-7.4%	74,743	-2.7%
Tower side pump	9,470	9,470	0.0%	2,132	77.5%	4,232	55.3%
Tower fan	10,098	10,098	0.0%	4,796	52.5%	7,076	29.9%
Regeneration device	1,917	2,755	-43.7%	10,489	-447.1%	3,770	-96.6%

Based on the above analysis, it can be indicated that: the energy saving potential of the cooling season is significantly higher than that of the heating season (14.8% Vs. 4.7%). This can be explained as follows:
1) Since the cooling capacity of the tower is much larger than its heating capacity, the HTHP is usually sized according to the winter condition to meet both cooling and heating demands. As a result, the tower has redundant cooling capacity in full load and the redundancy increases with the decrease of load.

2) As shown in Fig. 5, the cooling season has higher percentage of low part load ratio than the heating season, which means the HTHP system operating in cooling mode is easier to deviate from the designed condition.

3) The energy consumption of the regeneration device in heating season shows the opposite tendency with that of the pumps and fans, which significantly reduces the total energy saving potential.

4.4.2. Typical day analysis

In order to further identify how energy saving of Approach 3 was achieved at different seasons, we run the physics-based model with the optimal control variables in two typical days and analyzed their thermodynamic performance. A typical summer day (July 30th), and a typical winter day (January 26th) were selected.

Fig. 9 (a) presents the weather data of the selected summer day, whose dry-bulb temperature ranges from 28.9°C to 35.2°C, and wet-bulb temperature is from 25.2°C to 26.6°C. The cooling load of the summer day varies from 229.3 kW to 362.4 kW. The part load ratios (PLRs) of the three heat pumps are demonstrated in Fig. 9 (b) and (c). As indicated in Section 3.2, the baseline adopts the conventional control strategy, in which the heat pumps are sequential controlled and the previous on-line ones are required to run with full load. For Approach 3, it shows that its better to operate all the on-line heat pumps with identical lower PLRs.
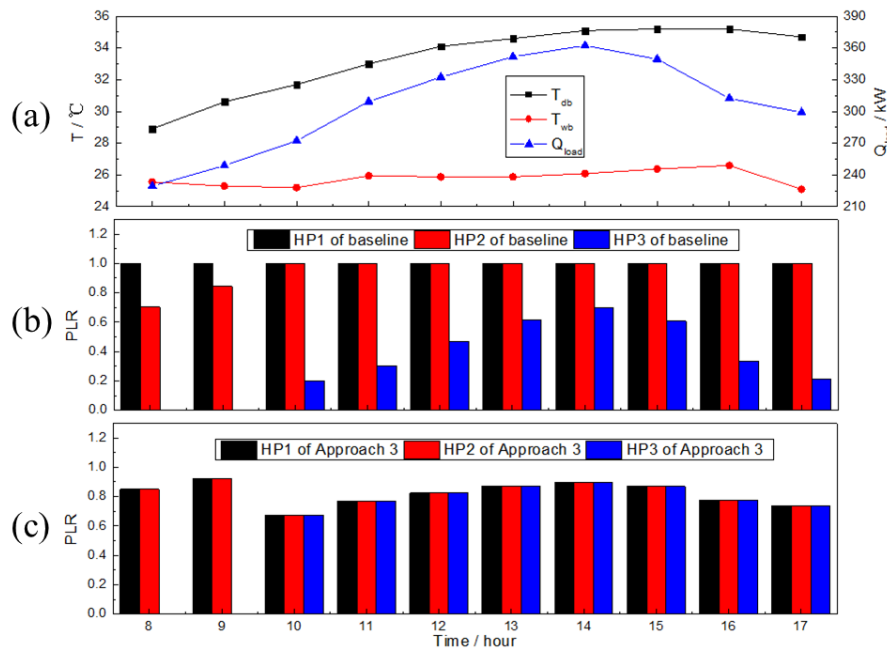

Fig. 9. Performance of the heat pumps for a summer day (a) weather data and building load; (b) PLR of baseline; (c) PLR of Approach 3

Fig. 10 (b) presents the optimal approaches and ranges of Approach 3, which are compared with the baseline. For the baseline, the mean approach and range of the condenser water are only 1.4°C and 3.2°C, respectively. Both the two values are much lower than those of the conventional cooling towers, whose designed approach and range are around 4°C and 5°C. As demonstrated in Fig. 10 (c), the tower of baseline rejects more latent heat from ambient than Approach 3 by higher air and condenser water flow rates. However, the direction of sensible heat transfer is

changed as the dry-bulb temperature rises. Thus, the total heat rejection capacity of the tower increases slowly with the increasing air and condenser water flow rates. As expected, the air and condenser water flow rates are reduced to save energy consumption of fans and pumps in Approach 3. The mean approach increases from 1.4°C to 2.9°C and range increases from 3.2°C to 4.8°C, respectively. As a result, the power consumption of pumps and fans have significantly reductions of 64.0% and 80.2%, as shown in Fig. 11. The side effect of the reductions in air and condenser water flow rates is that the mean condenser water supply temperature increases from 27.1°C to 28.7°C, which increases the power use of heat pumps slightly by 7.3%. For the entire system, an energy saving ratio of 12.8% is achieved by Approach 3.

It is noted that the settings of approach and range in Approach 2 is quite close to the optimal ones in Approach 3 for the studied typical day. This is the reason that Approach 2 also shows a considerable energy saving ratio.
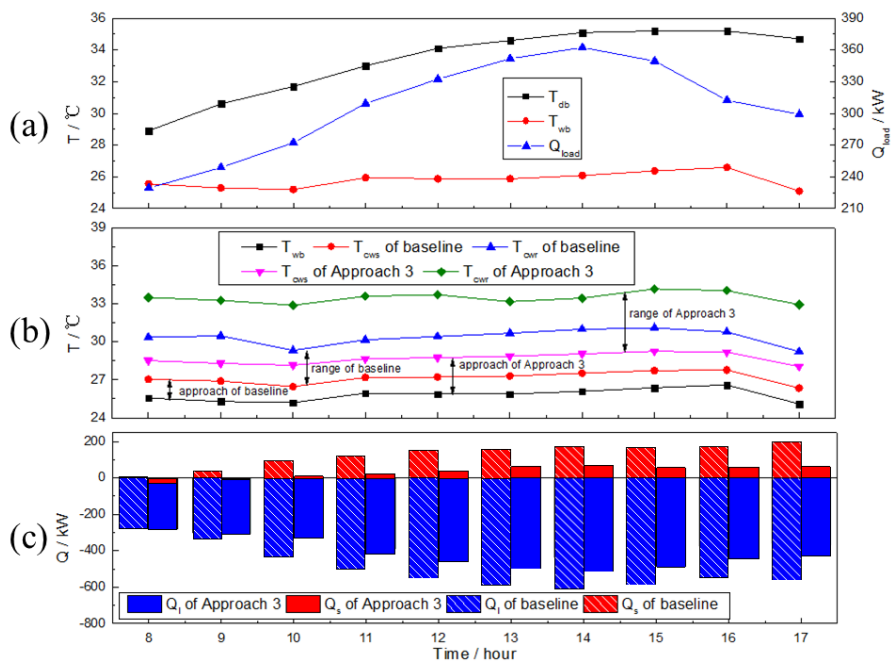

Fig. 10. Performance of the heating towers for a summer day (a) weather data and building load (b) approach and range (c) heat and mass transfer capacities of the tower
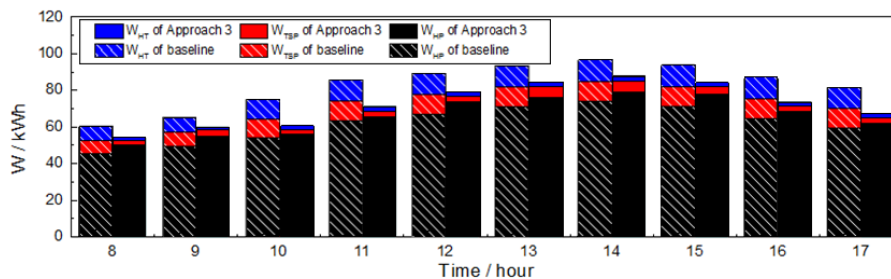

Fig. 11. Energy consumption of different components in a summer day

Fig. 12 presents the performance of the heat pumps for a winter day. The dry-bulb temperature of the selected winter day ranges from -3.8°C to 8.0°C, and its wet-bulb temperature varies from -4.0°C to 4.1°C, as shown in Fig.

12 (a). The building load are inverse to the changing dry-bulb temperature, varying from 198.0 kW to 280.7 kW. Fig. 12 (b) and (c) demonstrates the PLRs of the heat pumps of baseline and the optimal load distribution of Approach 3. Similar to that in the summer day, the Approach 3 also runs all three heat pumps at the same low PLR.
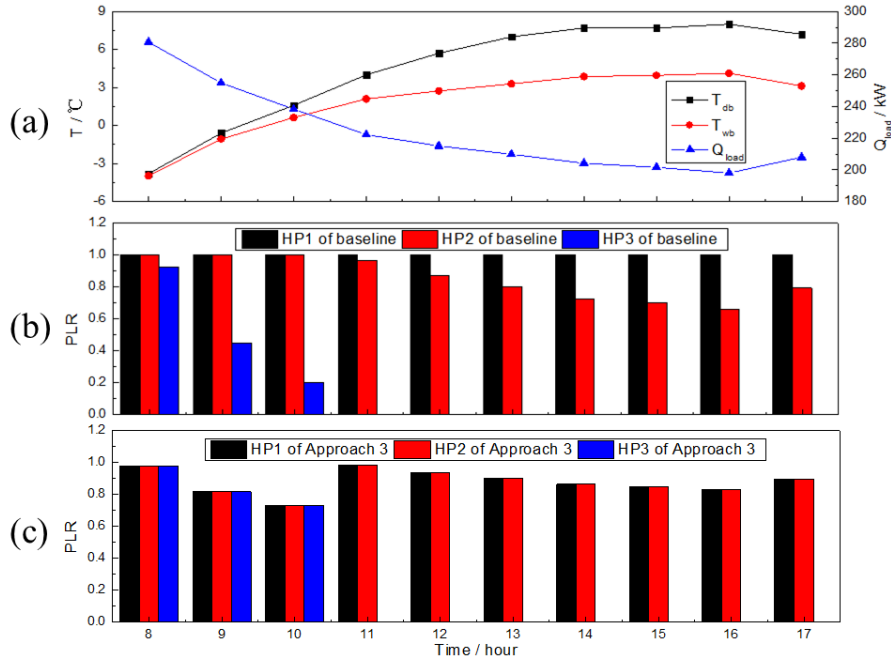

Fig. 12. Performance of the heat pumps for a winter day (a) weather data and building load (b) PLR of baseline (c) PLR of Approach 3

Fig. 13 presents the tower performance of baseline and Approach 3, including approach, range, sensible and latent heat transfer capacities. In the first five hours from 8:00 to 13:00, the heating tower absorbs both sensible and latent heat from ambient, as shown in Fig. 13 (c). In this condition, the mean approach and range of the baseline are 2.97°C and 1.65°C, and those of Approach 3 are 4.29°C and 2.51°C respectively. The lower air and solution flow rates of Approach 3 lead to smaller heat and mass transfer coefficients, as indicated in Eqs.(31) and (32). In order to provide enough energy to the heat pumps, the solution temperature drops to enhance the heat and mass transfer potential difference between air and solution. So, there is only little difference between the total heat transfer capacities of the baseline and Approach 3. But the energy consumption of heat pumps in Approach 3 has a slight increase of 7.0%, due to the lower solution supply temperature (lower evaporating temperature leads to lower COP of heat pumps), as shown in Fig. 14. On the other hand, the energy use of the pumps and fans in Approach 3 have significant reductions of 74.3% and 50.8%, compared with those in the baseline. Summing up the energy consumption of all the components, an energy saving ratio of 5.8% for the HTHP system is achieved by Approach 3.

For the last five hours from 13:00 to 18:00, the heating tower runs into the self-regeneration process, in which the tower absorbs sensible heat and rejects latent heat, as shown in Fig. 13 (c). In this condition, the enhancement of the heat and mass transfer capacities of heating tower not only improves the performance of heat pumps but also

reduces the energy consumption of the regeneration device. Thus, in Approach 3, the pumps run in about 80% speed, and the fans run almost in full speed to enhance the heat and mass transfer process, which is totally different with the first five hours. As a result, the energy saving ratios for pumps and fans are 43.1% and 0.7% while the heat pumps and regeneration device cost more power of 1.9% and 28.0% than the baseline. For the entire system, Approach 3 only saves 0.4%. In addition, Approach 2 that adopts low air and solution flow rates with fixed high approach and range does not make the most of the self-regeneration process and costs even more energy than the baseline.
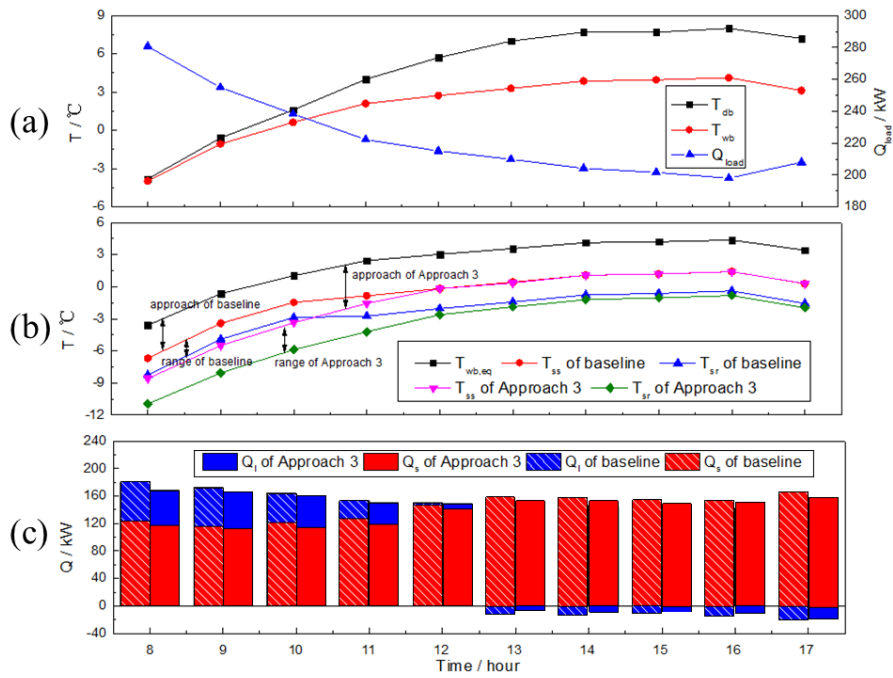

Fig. 13. Performance of the heating towers for a winter day (a) weather data and building load (b) approach and range (c) heat and mass transfer capacities of the tower
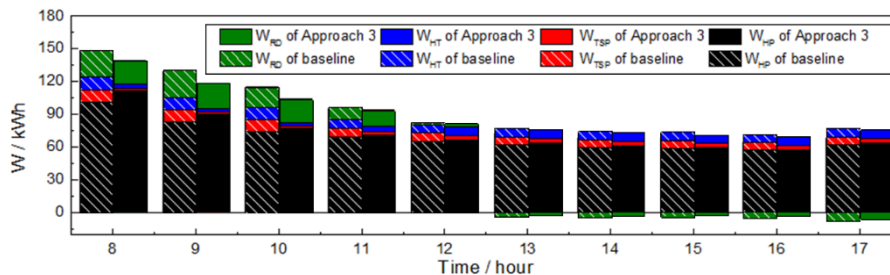

Fig. 14. Energy consumption of different components in a winter day

5. Conclusion

In order to minimize the energy consumption of the HTHP system in both cooling and heating modes, a model-based optimization method was proposed. The physics-based model was developed based on an existing HTHP.

Then, the ANN models were developed with the big data generated by the physics-based model. Based on the ANN models, the model-based optimization was performed by adopting genetic algorithm. The annual energy savings of the proposed approach were compared with three commonly used control strategies via a case study. The main conclusions are summarized as follows:

1) The physics-based model developed in this study has high accuracy, whose average error is less than 3.5% compared with the experiments. The ANN models trained and validated by the big data provided by the physics-based model, are found to be to be highly accurate (within 1% relative errors) and computationally efficient (about 300 times faster than the physics-based model), which makes the model-based optimization viable in the practice.

2) The optimal load distribution approach (Approach 1) achieves 2.7% and 1.6% energy savings in cooling and heating seasons, respectively due to the efficiency improvement of heat pumps in part load.

3) The fixed approach and range strategy (Approach 2) can save 11.4% power consumption in cooling season since the settings of approach and range in Approach 3 is quite close to the optimal ones in Approach 3. However, it costs even more energy (1.4%) than the baseline in the heating season. Because it does not make the most of the self-regeneration process with fixed high approach and range.

4) Taking the compressor speed, tower side pump speed, and tower fan speed as independent control variables, Approach 3 shows the highest energy saving ratio (14.8% energy saving in cooling season, and 4.7% energy saving in heating season).

5) The energy saving potential of cooling season is much higher than that of the heating season, which can be explained by the following three reasons: first, sizing the HTHP according to the winter condition can lead to the problem of mismatching in summer conditions; second, the cooling season has higher percentage of low part load ratio than the heating season; third, the self-regeneration process in heating season makes the regeneration device has opposite tendency with the pumps and fans in energy consumption.

Acknowledgement

Nomenclature

A	heat exchange area, m^2	λ	thermal conductivity coefficient, $W\ m^{-1}\ K^{-1}$
A_{th}	geometric throat area of the thermostatic expansion, m2	π	regression coefficient
c	regression coefficient	ρ	density，$kg\ m^{-3}$

C_D	constant mass flow coefficient	τ	approach of condenser water or solution, ℃
COP	coefficient of performance	Ψ	correction factor
C_p	specific heat capacity，kJ kg^{-1} K^{-1}	ω	humidity ratio，kg kg^{-1}
d	diameter of tube, m	**Subscript**	
EER	energy efficiency ratio	a	air
G	mass flow flux，kg m^{-2} s^{-1}	c	condenser
h	enthalpy, kJ kg^{-1}	$CHWS / CHWR$	supply / return chilled water
h_c	heat transfer coefficient of tower，W m^{-2} K^{-1}	$comp$	compressor
h_d	mass transfer coefficient of tower，g m^{-2} s^{-1}	CWS / CWR	supply / return condenser water
K	heat exchange coefficient, kW m^{-2} ℃$^{-1}$	db	dry-bulb
$LMTD$	logarithmic mean temperature difference, ℃	e	evaporator
M	mass flow rate, kg s^{-1}	g	gas phase
m	mass flow rate in one element, kg s^{-1}	HP	heat pump
N	rotation speed, Rev. min^{-1}	HT	Heating tower
P	pressure, Pa	HWS / HWR	supply / return hot water
Pr	Prandtl number，/	i	inlet or inner
Q	heat transfer capacity，kW	l	liquid phase
q	heat flux, W m^{-2}	m	mean value of the inside and outside
Q_l	latent heat transfer capacity of heating tower，kW	o	outlet or external
Q_s	sensible heat transfer capacity of heating tower，kW	R	refrigerant
r	vaporization latent heat，kJ kg^{-1}	$rated$	rated speed
R	Resistance of heat transfer, m^2 K W^{-1}	RD	regeneration device
Re	Reynolds number，/	s	solution
T	temperature, ℃	SS / SR	supply / return solution
u	dynamic viscosity, N s m^{-2}	TSP	tower side pump
W	power consumption, kW	USP	user side pump
x	dryness of refrigerant，/	v	vaper
X	mass concentration of solution，/	VFD	variable frequency drive
Greek symbols		w	water
$\triangle T$	range of condenser water or solution, ℃	$wall$	wall of tube
α_w	specific area of the packing，m^2 m^{-3}	wb	wet-bulb
δ	thickness of the tube wall, m	wb,eq	equivalent wet-bulb
ε	correction factor		

References

[1] Stanford H W. HVAC water chillers and cooling towers: fundamentals, application, and operation [M]. CRC Press, 2016.

[2] Fujita T, Kawahara K. Thermal characteristics of heating towers[J]. Transactions of the Japan Society of Refrigerating and Air Conditioning Engineers, 2012, 6: 275-284.

[3] Huang S, Lv Z, Liang C, et al. Experimental study of heat and mass transfer characteristics in a cross-flow heating tower [J]. International Journal of Refrigeration, 2017, 77: 116-127.

[4] Huang S, Zuo W, Lu H, et al. Performance comparison of a heating tower heat pump and an air-source heat pump: A comprehensive modeling and simulation study[J]. Energy conversion and management, 2019, 180: 1039-1054.

[5] Huang S, Ye Y, Han X, et al. Performance evaluation of heating tower heat pump systems over the world[J]. Energy Conversion and Management, 2019, 186: 500-515.

[6] Wei X, Li N, Peng J, et al. Modeling and Optimization of a CoolingTower-Assisted Heat Pump System[J]. Energies, 2017, 10(5): 733.

[7] Cheng J, Zou S, Chen S. Application Research on the Closed-loop Heat-source-Tower Heat Pump Air Conditioning System in Hot-summer and Cold-winter Zone [J]. Procedia Engineering, 2015, 121: 922-929.

[8] Yu F W, Chan K T. Optimization of water-cooled chiller system with load-based speed control [J]. Applied Energy, 2008, 85: 931-950.

[9] Huang S, Malara A C L, Zuo W, et al. A Bayesian network model for the optimization of a chiller plant's condenser water set point [J]. Journal of Building Performance Simulation, 2016, 11: 36-47.

[10] Huang S, Zuo W, Sohn M D. Amelioration of the cooling load based chiller sequencing control [J]. Applied Energy, 2016, 168: 204-215.

[11] Huang S, Zuo W, Sohn M D. Improved cooling tower control of legacy chiller plants by optimizing the condenser water set point [J]. Building and Environment, 2017, 111: 33-46.

[12] Liu Z, Tan H, Luo D, et al. Optimal chiller sequencing control in an office building considering the variation of chiller maximum cooling capacity [J]. Energy and Buildings, 2017, 140: 430-442.

[13] Thangavelu S R, Myat A, Khambadkone A. Energy optimization methodology of multi-chiller plant in commercial buildings [J]. Energy, 2017, 123: 64-76.

[14] Xu Z Y, Wang R Z. Comparison of CPC driven solar absorption cooling systems with single, double and variable effect absorption chillers[J]. Solar energy, 2017, 158: 511-519.

[15] Xu Z Y, Wang R Z. Simulation of solar cooling system based on variable effect LiBr-water absorption chiller[J]. Renewable Energy, 2017, 113: 907-914.

[16] Chen C-L, Chang Y-C, Chan T-S. Applying smart models for energy saving in optimal chiller loading [J]. Energy and Buildings, 2014, 68: 364-371

[17] Yu F W, Chan K T. Optimization of water-cooled chiller system with load-based speed control [J]. Applied Energy, 2008, 85: 931-950.

[18] Shan N, Yin Y, Zhang X. Study on performance of a novel energy-efficient heat pump system using liquid desiccant [J]. Applied Energy, 2018, 219: 325-337.

[19] Karami M, Wang L. Particle Swarm optimization for control operation of an all-variable speed water-cooled chiller plant [J]. Applied Thermal Engineering, 2018, 130: 962-978.

[20] Xue X, Sun T, Shi W, et al. A Novel Method of Minimizing Power Consumption for Existing Chiller Plant [J]. Procedia Engineering, 2017, 205: 1959-1966.

[21] Wen X, Cao Q, Yu P, et al. Energy-saving analysis and experimental study of a new heat-source tower solution regeneration system[J]. CIESC Journal, 2018, 69(5): 2226-2232.

[22] Wen X, Cao Q, Yu P, et al. Experimental Research on a Novel Solution Regeneration System for Heat Source tower Based on Vacuum Boiling and Condensation[J]. ES Energy & Environment, 2018, 2:1-7.

[23] AHRI. AHRI Standard 540, Performance rating of positive displacement refrigerant compressors and compressor units [S].Air-Conditioning, Heating, and Refrigeration Institute, 2015.

[24] Park N, Shin J, Chung B. A new dynamic heat pump simulation model with variable speed compressors under frosting conditions [C]//8th International Conference on Compressors and their Systems. 2013: 681-696.

[25] Cuevas C, Lebrun J. Testing and modelling of a variable speed scroll compressor [J]. Applied Thermal Engineering, 2009, 29: 469-478.

[26] Eames I W, Milazzo A, Maidment G G. Modelling thermostatic expansion valves [J]. International Journal of Refrigeration, 2014, 38: 189-197.

[27] Wei X, Li N, Peng J, et al. Analysis of the effect of the CaCl2 mass fraction on the efficiency of a heat pump integrated heat-source tower using an artificial neural network model [J]. Sustainability, 2016, 8: 410.

[28] Mohurd. GB 50736-2012, Design code for heating ventilation and air conditioning of civil buildings [S].China Architecture and Building Press, 2012.

[29] Copeland select software [DB/OL]. https://climate.emerson.com/en-gb/tools-resources/copeland-select-software.

[30] Huang S, Lv Z, Zhang X, et al. Experimental investigation on heat and mass transfer in heating tower solution regeneration using packing tower[J]. Energy and Buildings, 2018, 164: 77-86.